Facile synthesis of CuO nanoribbons/rGO nanocomposites for high-performance formaldehyde gas sensor at low temperature

Zhichen Lu[1], Zhenren Ma[1], Peng Song[1,*], and Qi Wang[1,*]

[1] *School of Materials Science and Engineering, University of Jinan, Jinan 250022, China*

ABSTRACT

In the present study, the CuO nanoribbons/reduced graphene oxides (rGO) nanocomposites have been successfully synthesized via a water-bath heating method. A series of characterizations manifest that CuO nanoribbons with average width of 100–200 nm are uniformly dispersed on the surface of rGO sheet. Meanwhile, the specific surface area and average pore size of as-obtained nanocomposites are 31.32 m^2/g and 6.4 nm, respectively. More importantly, the as-obtained CuO nanoribbons/rGO nanocomposites exhibit superior gas-sensing property for ultra-low concentration formaldehyde (HCHO) detections at low temperature, which due to the mesoporous structure, large specific surface area, and excellent charge carriers transport properties. The response value of the CuO nanoribbons/rGO nanocomposites sensors to 1 ppb HCHO gas is about 22% at the optimal operating temperature of 80 °C with the extremely fast response and recovery time of both 1 s. It is expected that CuO nanoribbons/rGO nanocomposites with remarkable sensing performance have a wide application prospect in future development on monitoring and detecting HCHO at low temperature.

1 Introduction

In recent year, the rapid development of science and technology has promoted the development of the country and society, but it has brought about environmental problems, especially the problem of gas pollution. Gas pollution is one of the important environmental pollution problems, producing serious threats to human health and security [1]. Mostly, formaldehyde (HCHO), carbon oxides (CO_x), nitrogen oxides (NO_x), and other toxic and harmful substances cause air pollution [2–5]. Among them, HCHO is widespread generated from chemical factories, packing house, and explosives [6–9]. And HCHO, as a toxic gas, can harm people's health and even cause death. Therefore, in order to protect human health, highly selective and rapid detection of gas sensors is needed to detect HCHO at low concentrations in homes and industries.

Address correspondence to E-mail: mse_songp@ujn.edu.cn; mse_wangq@ujn.edu.cn

Metal oxide semiconductors (MOSs) have the advantages of fast response speed and good selectivity. Therefore, the MOSs have attracted much attention in the detection of harmful gases. Among the MOSs, the band gap of copper oxide (CuO) is about 1.2 eV, which is a typical p-type metal oxide semiconductor [10]. And CuO has many excellent features, such as easy availability, low cost, easy production, and so on. Therefore, CuO is widely used in gas sensing. In particular, one-dimensional (1D) CuO nanoribbons have been widely studied due to its large specific surface area. For example, Gou et al. reported that CuO nanoribbons had good gas-sensing properties for HCHO [11]. However, CuO has the disadvantages of high operation temperature [12]. In especial, the operation temperature of pure CuO is 200–450 °C. Meanwhile, high operation temperature is not convenient for the application of pure CuO in daily life, which will make its work unstable and reduce its service life.

As a promising room-temperature gas-sensing material, reduced graphene oxide (rGO) has unique two-dimensional atomic thickness structure and excellent physical properties, such as large specific surface area and high electron mobility at room temperature, which meets the basic requirements of room-temperature gas detection for sufficient RT conductivity and high surface reactivity. For examples, Zeng et al. reported that rGO exhibited good gas sensibility to 20 ppm NO_2 at the room temperature [13]. Next, the rGO can improve the stability of nanomaterials [14, 15]. In order to improve the gas-sensing performance, the rGO/MOSs nanocomposites were formed by metal oxide semiconductor composite on reduced graphene oxide nanosheets [16–18]. With further research, the gas-sensing property of the rGO/MOSs nanomaterials was improved at low temperature. For instance, Chao et al. found that the rGO/In_2O_3 nanocomposites had better gas-sensing performance for NO_2 at 50 °C [19]. Also, Yin et al. report that the Sn_3O_4/rGO nanocomposites detect HCHO gas-sensing performance at 150 °C [20]. However, studies have scarcely been investigated on the determination of HCHO at low temperature by CuO nanoribbons/rGO.

Herein, we report the design and preparation of novel CuO nanoribbons/rGO nanocomposites, in which CuO nanoribbons were uniformly dispersed on the surface of rGO nanosheets via a facile one-step water-bath heating path. Meanwhile, the gas-sensing properties of the CuO nanoribbons/rGO nanocomposites were studied. Through the analysis of gas-sensing data, the CuO nanoribbons/rGO nanocomposites have good gas sensitivity to HCHO. The CuO nanoribbons/rGO nanocomposites have good selectivity and fast response recovery time to HCHO because of rich active sites, high surface area, and excellent carrier transport performance. Therefore, the CuO nanoribbons/rGO nanocomposites synthesized in this experiment have a wide application prospect in HCHO detection.

2 Experimental

Graphene oxide (GO) was synthesized from natural graphite powder by a modified Hummers method [21–24]. In this experiment, the water-bath heating path for the preparation of new CuO nanoribbons/rGO nanocomposites was designed, as shown in Fig. 1. In a typical process, 100 mL of 0.01 M $CuCl_2$ solution was added into a 250 mL beaker, then 10 mL of 2.0 M NaOH solution was added to form a uniformly dispersed solution by magnetic stirring. Then, 10 mg of 1wt% GO was added to the above solution to disperse it in the solution. The 10 mL 0.6 M sodium citrate is added to reduce the $Cu(OH)_2$ to CuO and the GO to rGO, respectively. The resulting solution was reacted in a 55 °C water-bath heater for 5.5 h to obtain the brown solution. Then, the as-obtained solution was cooled to room temperature and precipitated. The precipitates were washed three times with deionized water and anhydrous ethanol, respectively. Subsequently, the as-obtained precipitate was freeze dried overnight at − 50 °C. Finally, CuO nanoribbons/rGO nanocomposites were prepared by annealing the precursor in argon atmosphere at a heating rate of 3 °C min^{-1} at 400 °C for 2 h.

The gas-sensing measurements were carried out using the WS-30A system (Winsen Technology Co. Ltd, Zhengzhou, China) via a static process, which was previously reported by our research team elsewhere [25]. The sensor can measure the response in air or target gas by monitoring the voltage on the reference resistor. The sensor response is defined as follows:

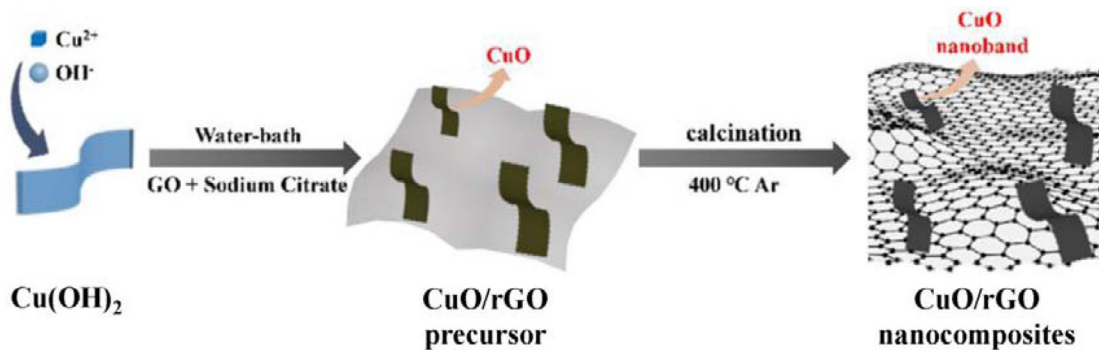$$Response = (R_{gas} - R_{air})/R_{air} \times 100\%, \qquad (1)$$

Fig. 1 The schematic of growth mechanism of CuO/rGO nanocomposites

where R_{air} and R_{gas} are the resistance of sensor in air and in the presence of the test gas, respectively [26–29].

3 Results and discussions

3.1 Compositional and morphological analysis

The crystal structure and phase composition of the CuO nanoribbons/rGO nanocomposites were studied by X-ray diffraction. Figure 2 shows the XRD patterns of pure CuO nanoribbons and CuO nanoribbons/rGO nanocomposites. All the peaks of CuO nanoribbons are corresponding to the cubic phase of CuO (JCPDS card No. 65-2309). It is found that the diffraction peak of the as-obtained CuO nanoribbons is very sharp and there is no other impurity peak. Therefore, it is proved that the as-

obtained CuO nanoribbons have good crystallinity and high crystal purity [30–33]. For the XRD pattern of CuO/rGO nanocomposites, the characteristic broad diffraction peak corresponding to rGO is not observed. The possible reason may be that the rGO content in the composite is relatively low, and the diffraction peaks of rGO are greatly suppressed by that of CuO because of their much lower intensity.

As shown in Fig. 3, the Raman spectra of CuO nanoribbons/rGO nanocomposites display four distinctive peaks at 1361.33 cm^{-1} in d-band, 1599.2 cm^{-1} in G-band, and 2656.01 cm^{-1} in 2D band [34]. The difference peak of 2D band was amplified from 2200 to 3300 cm^{-1}, as shown in the insertion diagram, which indicated that the prepared rGO had good morphology [35]. D/G-band strength ratio is often used to evaluate the ordering degree of graphite in carbon materials. The D/G-band strength ratio of CuO nanoribbons/rGO nanocomposites is 0.95, indicating that graphene has SP^2 hybrid structure
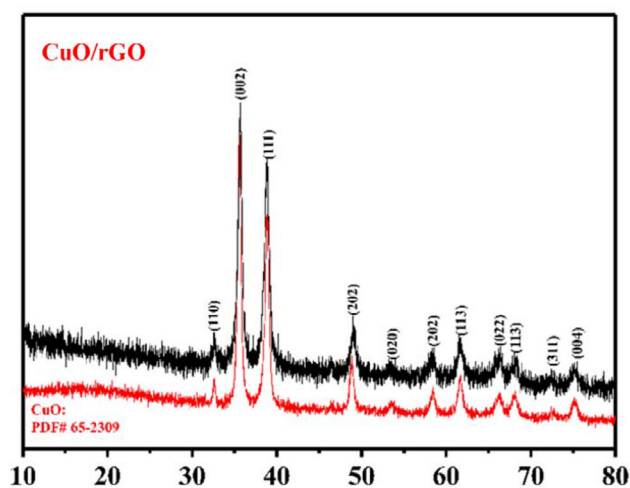

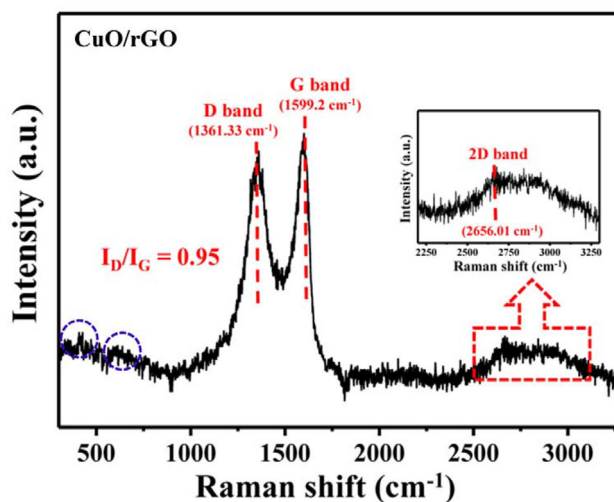**Fig. 2** XRD patterns of the as-obtained CuO and CuO/rGO nanocomposites

Fig. 3 Raman spectroscopy of CuO/rGO nanocomposites

[36]. Meanwhile, the peaks at 346 and 631 cm^{-1} appeared in the CuO/rGO nanocomposites are the characteristic modes of CuO [37]. The as-prepared sample is relatively darker due to absorption of light by the rGO, and hence, the Raman peaks associated to the stretching vibrations of short Cu–O bonds are weak.

The morphology and elemental composition of CuO nanoribbons/rGO nanocomposites were characterized by field emission scanning electron microscopy (FESEM) and energy dispersive spectrometer (EDS). FESEM images of CuO nanoribbons/rGO nanocomposites are shown in Fig. 4a–d. It can be found that CuO samples have ribbon-like nanostructures, which are uniformly distributed on the rGO substrates. The CuO nanoribbons/rGO nanocomposites samples were further characterized using EDS patterns to determine the elemental composition, as shown in Fig. 4e–h. The EDS result reveals the co-existence of C, Cu, and O. Thus, based on the results given by XRD, Raman, SEM, and EDS analysis, it can be undoubtedly concluded that CuO/rGO nanocomposites, with the feature of CuO nanoribbons anchoring uniformly on the surface of rGO sheets.

The structure and morphology of CuO nanoribbons/rGO nanocomposites were further analyzed by transmission electron microscopy (TEM). From the TEM images shown in Fig. 5a, b, it can be confirmed that ultrathin CuO nanoribbons are dispersed on rGO sheet. Meanwhile, Fig. 5c clearly shows the width size of CuO nanoribbons and the folded structure of rGO. It can be seen from the TEM image that the CuO nanoribbons with a width of about 100–200 nm are in close contact with the surface of rGO. In Fig. 5d, the HRTEM diagram of lattice fringes of CuO nanoribbons/rGO nanocomposites is shown, and the crystal plane spacing is about 0.25 nm. They can be attributed to the (002) crystal face of cubic CuO phase [38–40]. Through the above TEM analysis, CuO nanoribbons have no obvious agglomeration owing to the presence of rGO substrate and have the porous structure, which will improve the gas-sensing performance.

Subsequently, the surface areas and porous structures of CuO nanoribbons/rGO nanocomposites were characterized by N$_2$ adsorption and desorption measurements. As shown in Fig. 6, the adsorption isotherm of the sample is recognized as type IV based on Brunauer–Demin–Deming–Teller classification, indicating the existence of abundant mesoporous

structures [41]. The pore-size distribution curve shows that the corresponding pore sizes are centered at 6.4 nm. In addition, the large specific surface area of CuO nanoribbons/rGO nanocomposites is calculated to be 31.32 m^2/g. Therefore, due to its large specific surface area and mesoporous structure, the adsorption capacity of CuO nanoribbons/rGO nanocomposites is greatly improved, which also helps enhance the gas-sensing response.

The chemical state of the composite was further analyzed by X-ray photoelectron spectroscopy (XPS). The characteristic peaks of C, O, and Cu elements are clearly found in the CuO nanoribbons/rGO nanocomposites in Fig. 7a. Furthermore, Fig. 7b shows that two characteristic peaks with band energy at 962.9 eV and 944.3 eV correspond to Cu 2P$_{3/2}$ and Cu 2p$_{1/2}$ peaks, respectively [42]. In addition, Fig. 7c shows the C 1 s spectrum of three peaks, which can explain the C–C/C=C (284.9 eV) and C=O (285.5 eV) groups [43]. The dominant O 1 s peak at 538.8 eV belongs to the lattice oxygen of CuO nanoribbons (Fig. 7d). Due to the existence of two characteristic peaks of CuO in the sample, it indicates that CuO nanoribbons/rGO nanocomposites have been successfully synthesized [44].

3.2 Gas-sensing properties of the CuO/rGO nanocomposites

In order to determine the optimal operating temperature of CuO nanoribbons/rGO nanocomposites, the sensor response to 100 ppb HCHO was firstly examined in the temperature range of 35 to 280 °C. From the results of Fig. 8a, response of CuO nanoribbons/rGO nanocomposites first increases and then decreases with the increase of working temperature. The gas response of the sensor reaches the maximum value of 49% at 80 °C. Due to the remarkable electrical conductivity of CuO nanoribbons/rGO nanocomposites, the optimal working temperature is reduced. As shown in Fig. 8b, the sensor shows a favorable response to HCHO even at a very low concentration of 1 ppb, and the response increases with the increase of HCHO concentration. When the working temperature is 80 °C, the corresponding responses of CuO nanoribbons/rGO nanocomposites sensor are 22%, 26%, 30%, 36%, and 49% at different HCHO concentrations of 1, 5, 10, 50, and 100 ppb, respectively. In addition, the enlarged response–recovery curve to 1 ppb HCHO is inseted
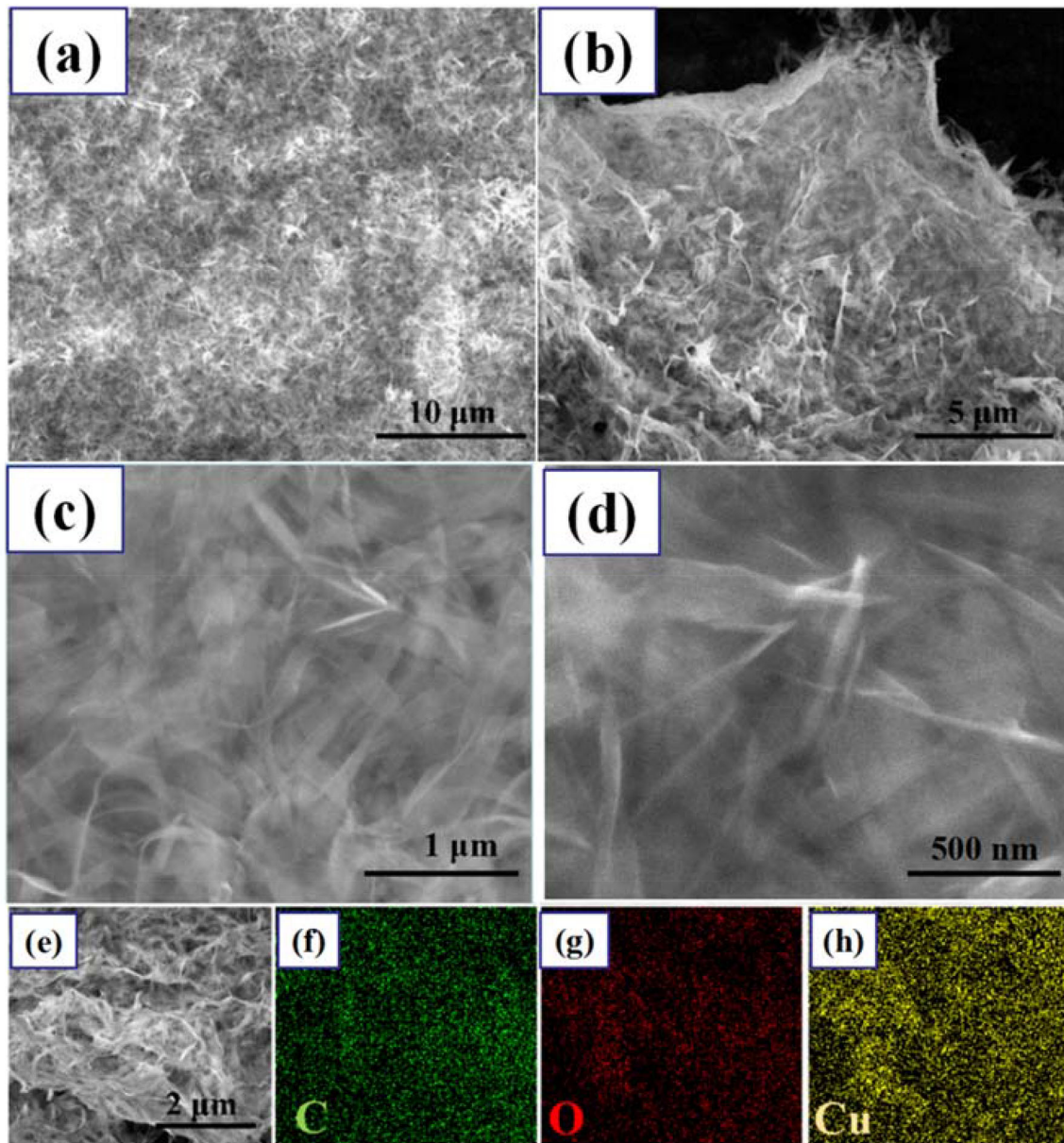
Fig. 4 SEM images of CuO/rGO (**a–d**), EDS images of CuO/rGO nanocomposites (**e–h**)

in Fig. 8b. It can be seen that the response of the sensor to 1 ppb HCHO is very fast, and the response time and recovery time are 1 s, respectively. Figure 8c shows that the sensor was tested three times in 100 ppb HCHO at the optimal operating temperature of 80 °C. The results show that the response of the sensor has no obvious change with good reproducible, indicating that the sensor has good stability in practical application [45]. Figure 8d shows that the response of the sensor to 100 ppb VOCs (such as NO$_2$, acetone, ethanol, toluene, methanol, and HCHO) was measured at the optimal operating

temperature of 80 °C. It is revealed that the response of the sensor to NO$_2$, acetone, ethanol, toluene, methanol, and HCHO is 2.5%, 2.3%, 1.5%, 3%, 3.5%, 3%, and 49%, respectively. The results show that the sensor has good selectivity for HCHO gas.

Table 1 shows the comparison of gas-sensing properties of CuO nanoribbons/rGO nanocomposites and other nanomaterials for formaldehyde. It can be clearly observed that the CuO nanoribbons/rGO nanocomposite sensor has excellent sensing properties compared with other nanomaterial sensors [46–49]. It can be inferred that the CuO nanoribbons/
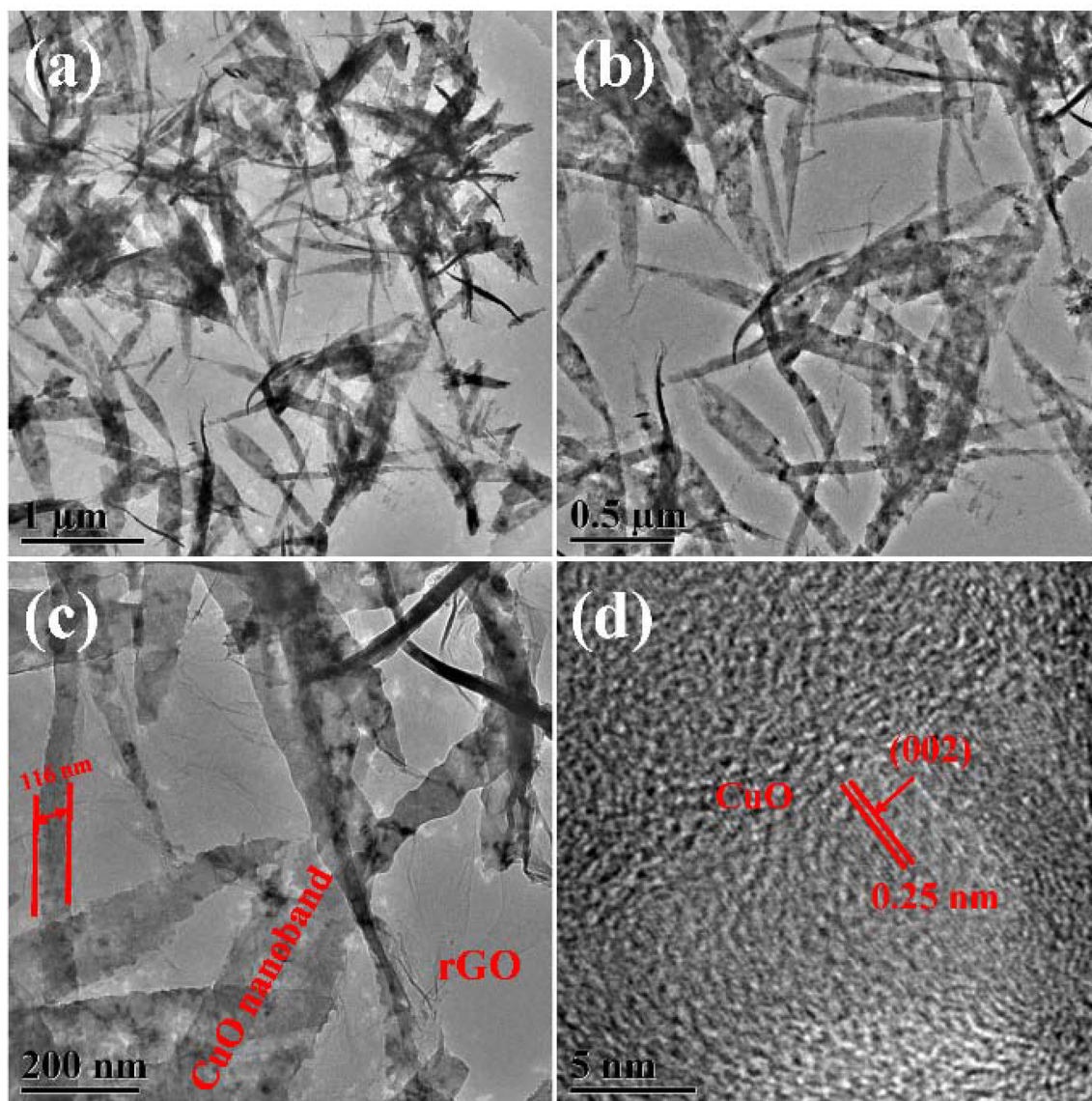
Fig. 5 **a**, **b** TEM image of the CuO/rGO nanocomposites; **c**, **d** high-resolution TEM image of CuO/rGO nanocomposites

rGO nanocomposite sensor has good gas-sensing performance for acetone and has potential application prospects in many fields.

3.3 Gas-sensing mechanism of the CuO/rGO nanocomposites

CuO nanoribbons/rGO nanocomposites also show p-type characteristics, because both rGO and CuO materials have p-type semiconductor characteristics when detecting HCHO gas [50, 51]. The electron transfer process on the surface of the sensor is shown in Fig. 9, which can better show the gas-sensing mechanism of CuO nanoribbons/rGO nanocomposites for HCHO detection. Through the flow equation, it can be found that when the sensor is exposed to air, oxygen molecules are adsorbed on the sensor surface, and oxygen molecules attract free electrons from the conduction band of CuO nanoribbons/rGO nanocomposites, leading to form of O^- and O_2^- species, thus, increasing the resistance of the sensor [52].

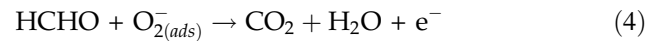$$O_{2(gas)} + e^- \rightarrow O_{2(ads)}^-. \tag{2}$$

In addition, from the following equation, when the CuO nanoribbons/rGO nanocomposites sensor is exposed to HCHO-reducing gas, the o-species on the
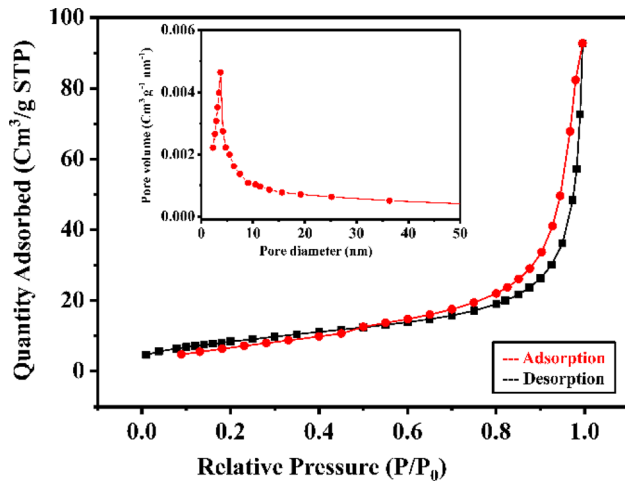
Fig. 6 XPS spectra of CuO/rGO nanocomposites: **a** wide XPS spectrum of CuO/rGO nanocomposites; **b** C 1 s spectrum; **c** Cu 2p spectrum; **d** O 1 s spectrum

sensor surface reacts with HCHO molecules, releasing electrons on the sensor surface. The trapped electrons are released into the conduction band and coupled with holes in the valance band. Thus, the concentration of holes decreases and the hole accumulation layer becomes thinner, leading to an overall decrease in the conductivity [53].

$$HCHO_{(gas)} \rightarrow HCHO_{(ads)} \tag{3}$$

$$HCHO + O^-_{2(ads)} \rightarrow CO_2 + H_2O + e^- \tag{4}$$

$$h^\bullet + e^- \rightarrow null \tag{5}$$

First, the above reactions show that CuO and rGO constitute P–P heterojunction. A large number of adsorbed oxygen ions are transformed through the surface of CuO nanoribbons/rGO nanocomposites, indicating that the balance of carrier concentration is broken. Second, two-dimensional nano-rGO has fast carrier mobility. So the electrons on the surface of rGO can be rapidly released into the conduction band of CuO to balance the carrier concentration.
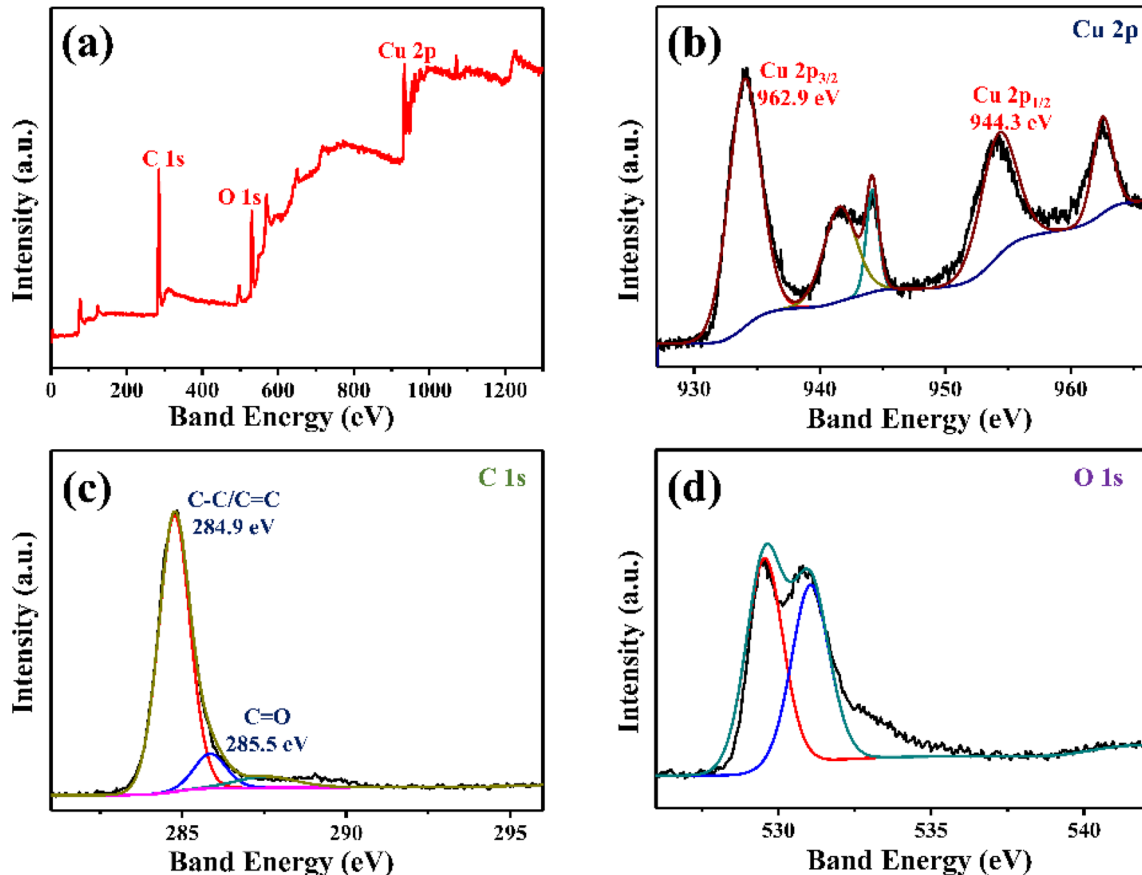
Fig. 7 N$_2$ adsorption–desorption isotherm curve and pore-size distribution plots (inset) of CuO/rGO nanocomposites
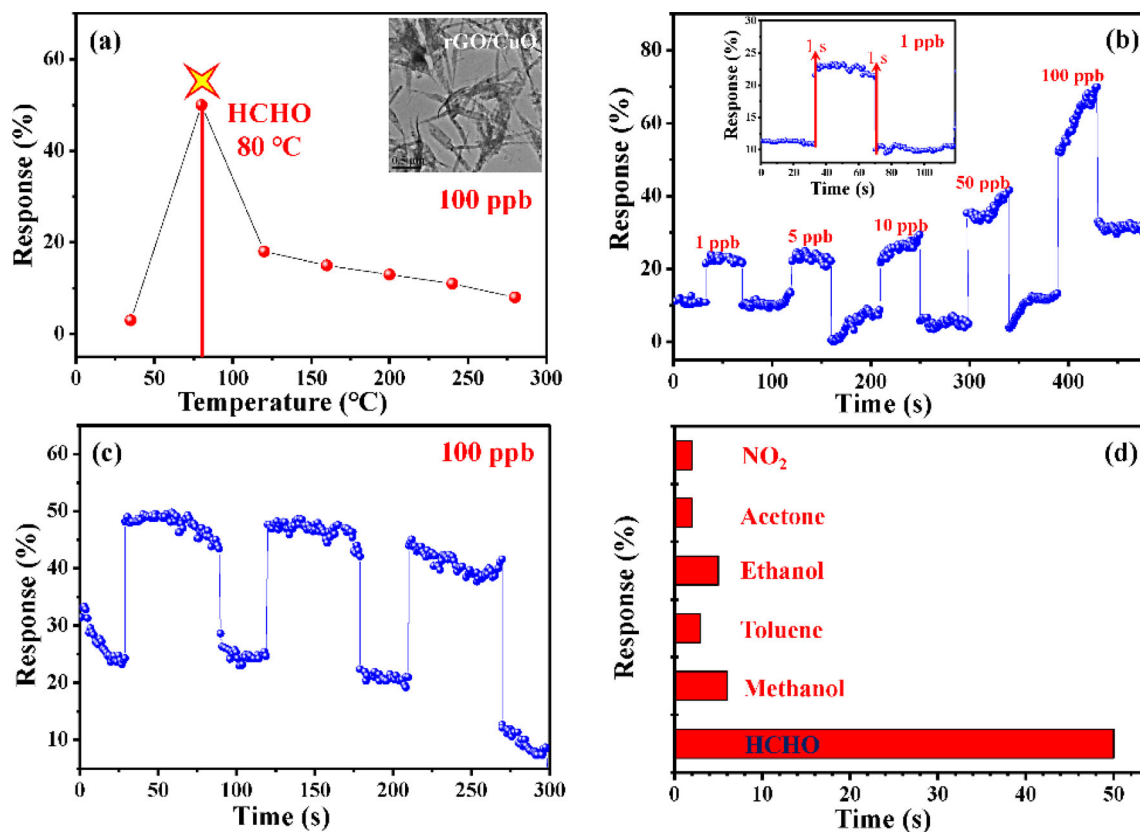
Fig. 8 a Optimum working temperature of CuO/rGO nanocomposites to 100 ppb HCHO. **b** Response and recovery curves of sensors were exposed to 1–100 ppb of HCHO at 80 °C and the response and recovery time to 1 ppb of HCHO at 80 °C (inset). **c** Response and recovery curves of sensors to the three cycle of 100 ppb HCHO at 80 °C. **d** Response of sensors ground on CuO/rGO nanocomposites to 100 ppb various gases at 80 °C

Table 1 Comparison of HCHO-sensing performances between CuO/rGO nanocomposites and previously reported sensing materials

Sensor material	T (°C)	HCHO (ppm)	Response (%)	Res/Rec (s/s)	Refs
CuO/rGO nanocomposites	RT	0.1	∼ 5	1/2	This work
CuO/rGO nanocomposites	80	0.1	49	1/1	This work
ZnO nanorod/rGO hybrid film	RT	10	5.5	34/500	[46]
SnO$_2$ nanoparticles/rGO hybrid	RT	5	4.6	46/95	[47]
SnO$_2$/CuO decorated graphene	RT	100	4.5	108/98	[48]
MoS$_2$/In$_2$O$_3$ nanocubes hybrids	RT	10	20.3	14/22	[49]

Subsequently, the adsorption rate of oxygen species and HCHO molecules can be increased due to the fast electron migration, which makes the detection of HCHO concentration in low concentration gas even to reach 1 ppb. Above all, the agglomeration of CuO nanoribbons was avoided by the matrix effect of rGO. Therefore, the CuO nanoribbon/rGO nanocomposites have a specific surface area up to 31.32 m^{2}g^{-1} and mesoporous structure. These properties make that CuO nanoribbons/rGO nanocomposites have high adsorption and diffusion capacity for HCHO molecules, which makes the response and recovery time of the sensor faster [54, 55]. In brief, the excellent gas-sensing properties of CuO nanoribbons/rGO nanocomposites are attributed to their fast electron mobility and mesoporous structure [56, 57].
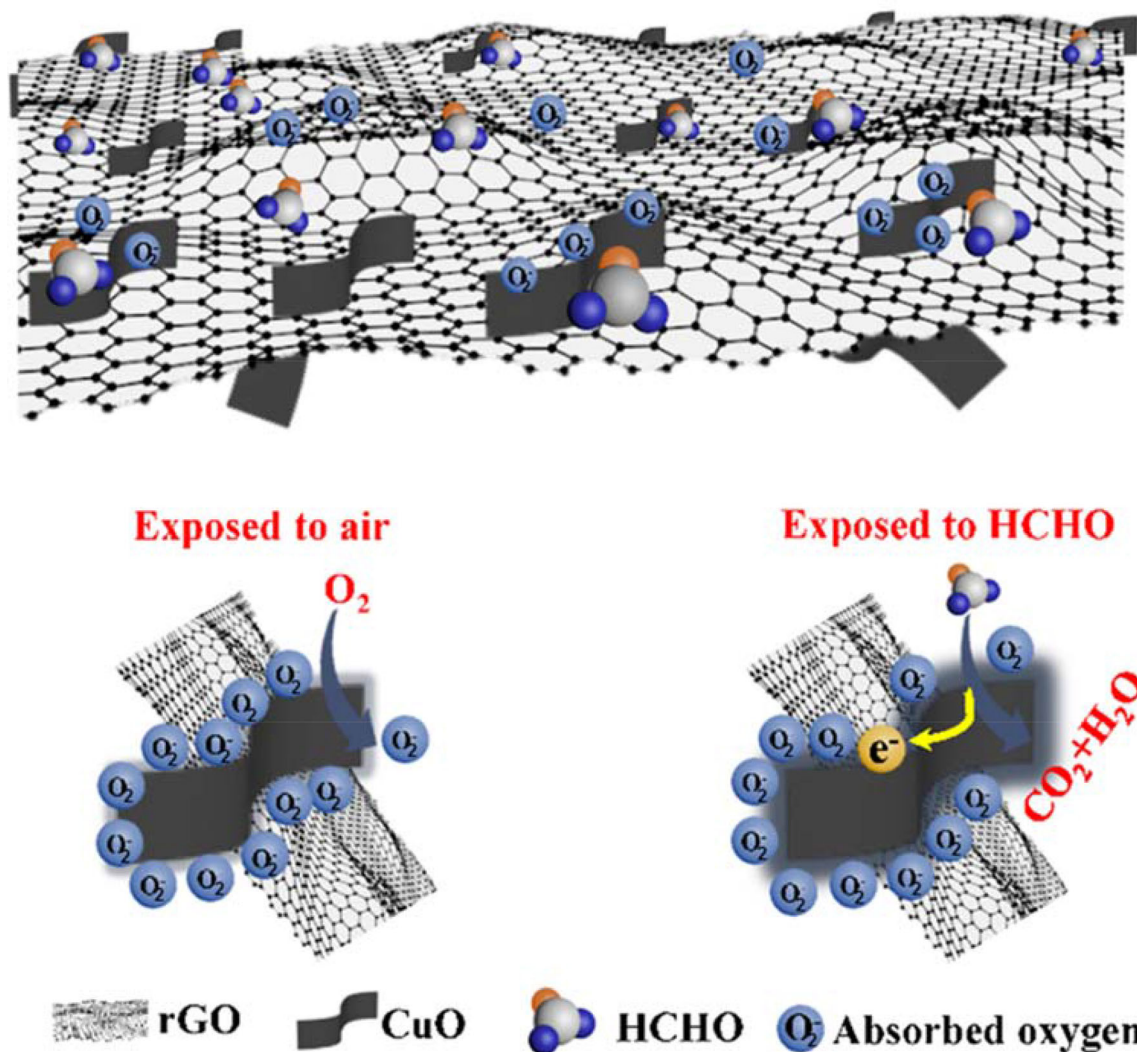
Fig. 9 The schematic of gas sensitivity mechanism of CuO/rGO nanocomposites

4 Conclusions

In conclusion, we have developed a simple experimental scheme for the synthesis of CuO nanoribbons/rGO nanocomposites for the HCHO detection. Through a series of characterization methods, the diameter of CuO nanoribbons is about 100–200 nm with the main pore diameter that is about 6.4 nm and the BET surface is analyzed to be 31.32 m^2/g. The results show that the sensor based on CuO nanoribbons/rGO nanocomposites has high response (about 22%), fast response, and recovery time (1 s and 1 s, respectively) and excellent selectivity for 1 ppb HCHO at 80 °C. The CuO nanoribbons/rGO nanocomposites with mesoporous structures provide more active sites and channels for the gas diffusion, promote the reaction between test gas molecules and oxygen ions, resulting in the improvement of the gas-sensing properties to HCHO gas.

References

1. K. Wetchakun, T. Samerjai, N. Tamaekong, C. Liewhiran, C. Siriwong, V. Kruefu, A. Wisitsoraat, A. Tuantranont, S. Phanichphant, Semiconducting metal oxides as sensors for environmentally hazardous gases. Sens. Actuators B: Chem. **160**, 580–591 (2011)

2. P. Song, D. Han, H.H. Zhang, J. Li, Z.X. Yang, Q. Wang, Hydrothermal synthesis of porous In_2O_3 nanospheres with superior ethanol sensing properties. Sens. Actuators B **196**, 434–439 (2014)

3. Y.S. Xu, J.Y. Xie, Y.F. Zhang, F.H. Tian, C. Yang, W. Zheng, X.H. Liu, J. Zhang, N. Pinna, Edge-enriched WS_2 nanosheets on carbon nanofibers boosts NO_2 detection at room temperature. J. Hazard. Mater. **411**, 125120 (2021)

4. W.W. Guo, Q.L. Zhou, J. Zhang, M. Fu, N. Radacsi, Y.X. Li, Hydrothermal synthesis of Bi-doped SnO_2/rGO nanocomposites and the enhanced gas sensing performance to benzene. Sens. Actuators B: Chem. **299**, 126959 (2019)

5. G.L. Lei, C.M. Lou, X.H. Liu, J.Y. Xie, Z.S. Li, W. Zheng, J. Zhang, Thin films of tungsten oxide materials for advanced gas sensors. Sens. Actuators B: Chem. **341**, 129996 (2021)

6. S. Zhang, P. Song, Z.B. Tian, Q. Wang, Template-free fabrication of hierarchical In_2O_3 hollow microspheres with superior HCHO-sensing properties. Phys. E. **99**, 152–159 (2018)

7. J.J. Sheng, C.T. Li, L.K. Zhao, X.Y. Du, L. Gao, G.M. Zeng, Efficient removal of HCHO from simulated coal combustion flue gas using CuO-CeO_2 supported on cylindrical activated coke. Fuel **197**, 397–406 (2017)

8. N.A. Travlou, E. Rodríguez-Castellón, T.J. Bandosz, Sensing of NH_3 on heterogeneous nanoporous carbons in the presence of humidity. Carbon **100**, 64–73 (2016)

9. B. Timmer, W. Olthuis, A. van den Berg, Ammonia sensors and their applications-a review. Sens. Actuators B: Chem. **107**, 666–677 (2005)

10. L. Hou, C.M. Zhang, L. Li, C. Du, X.K. Li, X.F. Kang, W. Chen, CO gas sensors based on p-type CuO nanotubes and CuO nanocubes: morphology and surface structure effects on the sensing performance. Talanta **188**, 41–49 (2018)

11. X.L. Gou, G.X. Wang, J. Yang, J.S. Park, D. Wexler, Chemical synthesis, characterisation and gas sensing performance of copper oxide nanoribbons. J. Mater. Chem. A **18**(9), 965–969 (2008)

12. K.D. Diao, J. Xiao, Z. Zheng, X.D. Cui, Enhanced sensing performance and mechanism of CuO nanoparticle-loaded ZnO nanowires: comparison with ZnO-CuO core-shell nanowires. Appl. Surf. Sci. **459**, 630–638 (2018)

13. J. Zhang, D.W. Zeng, H. Wang, Z.Y. Qin, A.M. Pang, C.S. Xie, Highly responsive chemical sensing on NO_2 at room temperature based on reduced porous graphene. Mater. Lett. **204**, 27–30 (2017)

14. L. Yin, H.B. Wang, L. Li, H. Li, D.L. Chen, R. Zhang, Microwave-assisted preparation of hierarchical CuO@rGO nanostructures and their enhanced low-temperature H_2S-sensing performance. Appl. Surf. Sci. **476**, 107–114 (2019)

15. S. Pourbeyram, R. Bayrami, H. Dadkhah, Green synthesis and characterization of ultrafine copper oxide reduced graphene oxide (CuO/rGO) nanocomposite. Colloid. Surf. A **529**, 73–79 (2017)

16. M. Mirmotallebi, A. Irajizad, Z.S. Hosseini, E. Jokar, Characterization of three-dimensional reduced graphene oxide/copper oxide heterostructures for hydrogen sulfide gas sensing application. J. Alloys Compd. **740**, 1024–1031 (2018)

17. S.L. Bai, X. Sun, N. Han, X. Shu, J.L. Pan, H.P. Guo, S.H. Liu, Y.J. Feng, R.X. Luo, D.Q. Li, A.F. Chen, rGO modified nanoplate-assembled ZnO/CdO junction for detection of NO_2. J. Hazard. Mater. **394**, 121832 (2019)

18. D.Z. Zhang, Z.L. Wu, X.Q. Zong, Flexible and highly sensitive H_2S gas sensor based on in-situ polymerized SnO_2/rGO/PANI ternary nanocomposite with application in halitosis diagnosis. Sens. Actuators B: Chem. **289**, 32–41 (2019)

19. Y. Chao, H.B. Lu, J.Z. Gao, Y. Zhang, Q.M. Guo, H.X. Ding, Y.T. Wang, F.F. Wei, G.Q. Zhu, Z.B. Yang, C.L. Wang, Improved NO_2 sensing properties at low temperature using reduced graphene oxide nanosheet–In_2O_3 heterojunction nanofibers. J. Alloys Compd. **741**, 908–917 (2018)

20. F.F. Yin, Y. Li, W.J. Yue, S. Gao, Z.X. Chen, Sn_3O_4/rGO heterostructure as a material for formaldehyde gas sensor with a wide detecting range and low operating temperature. Sens. Actuators B: Chem. **312**, 127954 (2020)

21. Q. Hao, T. Liu, J. Liu, Q. Liu, X. Jing, H. Zhang, G. Huang, J. Wang, Controllable synthesis and enhanced gas sensing properties of a single-crystalline WO_3-rGO porous nanocomposite. RSC Adv. **7**, 14192–14199 (2017)

22. P.S. Shewale, K.S. Yun, Synthesis and characterization of Cu-doped ZnO/rGO nanocomposites for room-temperature H_2S gas sensor. J. Alloys Compd. **837**, 155527 (2020)

23. J. Lee, A. Katoch, S. Choi, J. Kim, H.W. Kim, S.S. Kim, Extraordinary improvement of gas-sensing performances in SnO_2 nanofibers due to creation of local p-n heterojunctions by loading reduced graphene oxide nanosheets. ACS Appl. Mater. Interfaces **7**, 3101–3109 (2015)

24. R. You, D.D. Han, F.M. Liu, Y.L. Zhang, G.Y. Lu, Fabrication of flexible room-temperature NO_2 sensors by direct laser writing of In_2O_3 and graphene oxide composites. Sens. Actuators B: Chem. **277**, 114–120 (2018)

25. S. Zhang, P. Song, J. Zhang, H.H. Yan, J. Li, Z.X. Yang, Q. Wang, Highly sensitive detection of acetone using

mesoporous In_2O_3 nanospheres decorated with Au nanoparticles. Sens. Actuators B: Chem. **242**, 983–993 (2017)

26. Y.S. Xu, L.L. Zheng, C. Yang, X.H. Liu, J. Zhang, Highly sensitive and selective electronic sensor based on Co catalyzed SnO_2 nanospheres for acetone detection. Sens. Actuators B: Chem. **304**, 127237 (2020)

27. Z.J. Li, Y.Y. Liu, D.F. Guo, J.J. Guo, Y.L. Su, Room-temperature synthesis of CuO/reduced graphene oxide nanohybrids for high-performance NO_2 gas sensor. Sens. Actuators B: Chem. **271**, 306–310 (2018)

28. Y.S. Xu, W. Zheng, X.H. Liu, L.Q. Zhang, L.L. Zheng, C. Yang, N. Pinna, J. Zhang, Platinum single atoms on tin oxide ultrathin films for extremely sensitive gas detection. Mater. Horiz. **7**, 1519 (2020)

29. H.H. Yan, P. Song, S. Zhang, Z.X. Yang, Q. Wang, Facile synthesis, characterization and gas sensing performance of ZnO nanoparticles-coated MoS_2 nanosheets. J. Alloys Compd. **662**, 118–125 (2016)

30. H.W. Huang, Y. Liu, J.H. Wang, M.X. Gao, X.S. Peng, Z.Z. Ye, Self-assembly of mesoporous CuO nanosheets-CNT 3D-network composites for lithium-ion batteries. Nanoscale **5**, 1785–1788 (2013)

31. B.S. Ganesh, K. Peramaiah, J.C. Miriam, L.S. Kumar, A.K. Jeehyeong, N. Bernaurdshaw, Synergistic effect of sono-photocatalytic process for the degradation of organic pollutants using $CuO-TiO_2$/rGO. Ultrason. Sonochem. **50**, 218–223 (2019)

32. M. Liu, Z.Y. Wang, P. Song, Z.X. Yang, Q. Wang, Flexible MXene/rGO/CuO hybrid aerogels for high performance acetone sensing at room temperature. Sens. Actuators B: Chem. **340**, 129946 (2021)

33. A. Abulizi, G.H. Yang, J.J. Zhu, One-step simple sono-chemical fabrication and photocatalytic properties of Cu_2O-rGO composites. Ultrason. Sonochem. **21**, 129–135 (2014)

34. J.Y. Cai, W.J. Liu, Z.H. Li, One-pot self-assembly of Cu_2O/RGO composite aerogel for aqueous photocatalysis. Appl. Surf. Sci. **358**, 146–151 (2015)

35. H.Q. Ma, X. Sun, M.J. Wang, J.S. Zhang, Regenerable CuO/gamma-Al_2O_3-reduced graphene oxide adsorbent with a high adsorption capacity for dibenzothiophene from model diesel oil. Ind. Eng. Chem. Res. **57**, 10945–10955 (2018)

36. K. Wang, X.M. Dong, C.J. Zhao, X.Z. Qian, Y.L. Xu, Facile synthesis of Cu_2O/CuO/RGO nanocomposite and its superior cyclability in supercapacitor. Electrochim. Acta. **152**, 433–442 (2015)

37. S.K. Maji, N. Mukherjee, A. Mondal, B. Adhikary, B. Karmakar, Chemical synthesis of mesoporous CuO from a single precursor: structural, optical and electrical properties. J. Solid State Chem. **183**, 1900–1904 (2010)

38. R. Saravanan, S. Karthikeyan, V.K. Gupta, G. Sekaran, V. Narayanan, A. Stephen, Enhanced photocatalytic activity of ZnO/CuO nanocomposite for the degradation of textile dye on visible light illumination. Mater. Sci. Eng. C. **33**, 91–98 (2013)

39. H.J. Huang, J.Z. Zhang, L. Jiang, Z.G. Zang, Preparation of cubic Cu_2O nanoparticles wrapped by reduced graphene oxide for the efficient removal of rhodamine B. J. Alloys Compd. **718**, 112–115 (2017)

40. J.S. Kumar, M. Jana, P. Khanra, P. Samanta, T. Kuila, One pot synthesis of Cu_2O/RGO composite using mango bark extract and exploration of its electrochemical properties. Electrochim. Acta. **193**, 104–115 (2016)

41. X. Jie, D. Zeng, J. Zhang, K. Xu, J. Wu, B. Zhu, C. Xie, Graphene-wrapped WO_3 nanospheres with room-temperature NO_2 sensing induced by interface charge transfer. Sens. Actuators B: Chem. **220**, 201–209 (2015)

42. Z.Q. Yang, X.P. Hao, S.G. Chen, Z.Q. Ma, Z.H. Guo, Long-term antibacterial stable reduced graphene oxide nanocomposites loaded with cuprous oxide nanoparticles. J. Colloid Interface Sci. **533**, 13–23 (2019)

43. K. Sharma, K. Maiti, N.H. Kim, D. Hui, J.H. Lee, Green synthesis of glucose-reduced graphene oxide supported Ag-Cu_2O nanocomposites for the enhanced visible-light photo-catalytic activity. Compos. Part B-Eng **138**, 35–44 (2018)

44. S. Shahrokhian, S. Rezaee, Vertically standing Cu_2O nanosheets promoted flower-like PtPd nanostructures supported on reduced graphene oxide for methanol electro-oxidation. Electrochim. Acta. **259**, 36–47 (2018)

45. Q. Feng, X. Li, J. Wang, A.M. Gaskov, Reduced graphene oxide (rGO) encapsulated Co_3O_4 composite nanofibers for highly selective ammonia sensors. Sens. Actuators B: Chem. **222**, 864–870 (2016)

46. X. Li, J. Wang, D. Xie, J. Xu, R. Dai, L. Xiang, H. Zhu, Y. Jiang, Reduced graphene oxide/hierarchical flower-like zinc oxide hybrid films for room temperature formaldehyde detection. Sens. Actuators B: Chem. **221**, 1290–1298 (2015)

47. Z. Bo, M. Yuan, S. Mao, X. Chen, J. Yan, K. Cen, Decoration of vertical graphene with tin dioxide nanoparticles for highly sensitive room temperature formaldehyde sensing. Sens. Actuators B: Chem. **256**, 1011–1020 (2018)

48. D. Zhang, J. Liu, C. Jiang, A. Liu, B. Xia, Quantitative detection of formaldehyde and ammonia gas via metal oxide-modified graphene-based sensor array combining with neural network model. Sens. Actuators B: Chem. **240**, 55–65 (2017)

49. D. Zhang, C. Jiang, J. Wu, Layer-by-layer assembled In_2O_3 nanocubes/flower-like MoS_2 nanofilm for room temperature formaldehyde sensing. Sens. Actuators B: Chem **273**, 176–184 (2018)

50. S.Y. Gong, J.Y. Chen, X.F. Wu, N. Han, Y.F. Chen, In-situ synthesis of Cu$_2$O/reduced graphene oxide composite as effective catalyst for ozone decomposition. Catal. Commun. **106**, 25–29 (2018)

51. L.L. Sun, G.H. Wang, R.R. Hao, D.Y. Han, S. Cao, Solvothermal fabrication and enhanced visible light photocatalytic activity of Cu$_2$O-reduced graphene oxide composite microspheres for photodegradation of Rhodamine B. Appl. Surf. Sci. **358**, 91–99 (2015)

52. M.S. Park, K.H. Kim, M.J. Kim, Y.S. Lee, NH$_3$ gas sensing properties of a gas sensor based on fluorinated graphene oxide. Colloids Surf. A. **490**, 104–109 (2016)

53. Y.X. Li, D.Y. Deng, X.X. Xing, N. Chen, X. Liu, X.C. Xiao, Y.D. Wang, Formaldehyde detection: SnO$_2$ microspheres for formaldehyde gas sensor with high sensitivity, fast response/recovery and good selectivity. Sens. Actuators B **237**, 133–141 (2016)

54. Q. Wei, J. Sun, P. Song, J. Li, Z.X. Yang, Q. Wang, MOF-derived α-Fe$_2$O$_3$ porous spindle combined with reduced graphene oxide for improvement of TEA sensing performance. Sens. Actuators B Chem. **304**, 127306 (2020)

55. Z.R. Ma, P. Song, Z.X. Yang, Q. Wang, Trimethylamine detection of 3D rGO/mesoporous In$_2$O$_3$ nanocomposites at room temperature. Appl. Surf. Sci. **465**, 625–634 (2019)

56. X.Y. Wang, B.Y. Huang, X.F. Wu, D. Gu, X.G. Li, Enhanced ammonia sensing properties of rGO/WS$_2$ heterojunction based chemiresistive sensor by marginal sulfonate decoration. Sens. Actuators B **337**, 129776 (2021)

57. J. Zhang, X.H. Liu, G. Neri, N. Pinna, Nanostructured materials for room-temperature gas sensors. Adv. Mater. **28**, 795–831 (2016)

Publisher's Note Springer Nature remains neutral with regard to jurisdictional claims in published maps and institutional affiliations.